The cyclophilin A binding loop of capsid regulates the human TRIM5α sensitivity of non-pandemic HIV-1 Augustin P. Twizerimana¹, Daniel Becker², Shenglin Zhu¹, Tom Luedde¹, Holger Gohlke^{2, 3}, Carsten Münk^{1, #} ¹Clinic of Gastroenterology, Hepatology and Infectious Diseases, Medical Faculty, Heinrich Heine University Düsseldorf, Düsseldorf, Germany ²Institute for Pharmaceutical and Medicinal Chemistry, Heinrich Heine University Düsseldorf, Düsseldorf, Germany ³Forschungszentrum Jülich GmbH, Institute of Bio- and Geosciences (IBG-4: Bioinformatics), Jülich, Germany Classification: BIOLOGICAL SCIENCES, Microbiology Keywords: HIV-1, TRIM5, restriction factor, cyclophilin, capsid *Corresponding author: Carsten Münk, Clinic for Gastroenterology, Hepatology, and Infectiology, Medical Faculty, Heinrich-Heine-University Düsseldorf, Moorenstr. 5, 40225, Düsseldorf, Germany, Tel: +49 (0) 211-81-08720, carsten.muenk@med.uni-duesseldorf.de.

Abstract

31

32

33

34

35

36

37

38

39

40

41 42

43

44

45

46

47

The rather few cases of humans infected by HIV-1 N, O, or P raise the question of their incomplete adaptation to humans. We hypothesized that early post-entry restrictions may be relevant for the impaired spread of these HIVs. One of the best-characterized species-specific restriction factors is TRIM5α. HIV-1 M can escape human TRIM5α restriction by binding cyclophilin A (CYPA, also known as PPIA, peptidylprolyl isomerase A) to the so-called CYPA binding loop of its capsid protein. How non-M HIV-1s interact with huTRIM5α is illdefined. By testing novel full-length reporter viruses (Δ env) of HIV-1 N, O, P, and SIVgor, we found that, in contrast to HIV-1 M, the non-pandemic HIVs and SIVgor showed restriction by human TRIM5α. Work to identify capsid residues that mediate susceptibility to huTRIM5α revealed that capsid residue 88 in the capsid CYPA binding loop was important for such differences. There, HIV-1 M uses alanine to resist, while non-M HIV-1s have either valine or methionine, which avail them for huTRIM5α. Capsid residue 88 determines the sensitivity to TRIM5α in a so far unknown way. Molecular simulations indicated that capsid residue 88 can affect trans-to-cis isomerization patterns on the capsids of the viruses we tested. These differential CYPA usages by pandemic and non-pandemic HIV-1 suggest that the enzymatic activity of CYPA on the viral core might be important for its protective function against human TRIM5α.

48 49 50

Significance statement

51 52 53

54

55

56

57

58

59

Almost all cases of HIV-1 infections are caused by the pandemic HIV-1 M. The non-pandemic HIV-1s N, O, and P do not spread much in humans for unknown reasons. Human cells express TRIM5 α that restricts HIV-1. HIV-1 M evolved to escape this restriction by binding cyclophilin A to the viral core. Our data indicate that non-pandemic HIV-1s are sensitive to human TRIM5 α . In these viruses, cyclophilin A binding cannot protect against TRIM5 α , because its *trans/cis* isomerase enzymatic activity is reduced. Our data suggest that subtle changes induced by cyclophilin A in the capsid have a severe impact on viral infection.

60 61 62

63 64 65

66

67

68

69

70

71

72

73

74

75

76

Introduction

Human immunodeficiency virus 1 (HIV-1) is subdivided into four groups, the pandemic group M, and the non-pandemic groups N, O, and P (1). HIV-1 N was identified in 20 patients and HIV-1 P in two patients, circulating mostly (https://www.hiv.lanl.gov/). About 100.000 people have been infected with HIV-1 group O found in West and Central Africa with the highest prevalence in Cameroon, Gabun and Equatorial Guinea (2). HIV-1s are the evolutionary results of rare successful transmission events of simian immunodeficiency viruses (SIV) to humans. Group M and group N HIV-1s are derived from SIV of chimpanzees (SIVcpz), while group O and group P are the results of spillover of SIV of gorillas (SIVgor) (1, 3, 4). To halt retroviral replication, vertebrates use several cellular restriction factors (5–9). It is ill-defined whether the low prevalence of non-M HIVs is associated with the activity of antiviral factors such as the capsid-binding TRIM5α, which may limit their spread among humans.

77 78 79

80

TRIM proteins have a RING domain, a coiled-coil domain, and one to two B box domains (10). In addition, some TRIM proteins have a C-terminal PRYSPRY (B30.2) domain such as

in the alpha isoform of TRIM5, theTRIM5α, and TRIM25, or a cyclophilin A (CYPA) domain such as in the TRIM-Cyclophilin A (TRIMCyp) fusion proteins (11). The PRYSPRY or CYPA domains of TRIM5 proteins can bind retroviral cores. This binding initiates TRIM5 oligomerization to form higher-order oligomers around the conical core to affect the core integrity, and, thereby, impairs nuclear import and integration of the reverse-transcribed viral genome (11–13). The TRIM5 α binding to capsid can also result in intracellular signaling events for an extended viral restriction (11, 14). The anti-retroviral activity of TRIM5 proteins has been shown to mainly be PRYSPRY or CYPA domain-dependent (11). CYPA presence at the C-terminus of TRIM5 proteins is a result of the evolutionary retrotransposition of CYPA in some primates, like the Old World rhesus monkeys (Macaca mulatta) or the New World Aotus night/owl monkeys (15, 16). The antiretroviral activity of TRIM5α is thought to have formed a selective protective shield against the retroviral spread in vertebrate hosts (17, 18). As an example, human (hu) TRIM5α restricts infections by the horse lentivirus equine infectious anemia virus (EIAV) (19); in contrast, the pandemic HIV-1 M escapes the antiviral activity of huTRIM5 α by displaying binding sites in the viral core for CYPA (20, 21). The viral core is composed of about 1200 – 1500 capsid proteins in mostly hexameric organizations (22). Cellular CYPA and TRIMCyp bind the so-called CYPA binding loop of capsid formed by residues 85 to 93 (23-26). The CYPA - core interaction during the early phase of infection in the viral target cell is essential for its protective function against huTRIM5α(20). CYPA is also packaged by HIV virions, with less defined roles (27, 28). In virions, a CYPA-capsid stoichiometry of 0.1 and in in vitro assembled capsid tubes, a stoichiometry of $\sim 0.3-0.4$ was described (29-31). CYPA can influence many early steps of HIV infection (32–34) but the molecular mechanisms are not fully understood and may involve a trans/cis isomerization activity of CYPA and altered dynamics of the core (35, 36). Here we tested the antiviral property of human TRIM5α against non-M group HIVs but also SIVgor, identified viral determinants of sensitivity, and assessed the role of CYPA in the mechanism of TRIM5α to restrict HIVs.

Materials and methods.

Cells. CrFK and HEK293T cells were maintained in Dulbecco's high-glucose modified Eagle's medium (PAN Biotech, Aidenbach, Germany) with addition of 10% fetal bovine serum (FBS, PAN Biotech), 2 mM L-glutamine (PAN Biotech), 100 U/ml penicillin, and 100 μg/ml streptomycin (PAN Biotech). TRIM5α knockout U87-MG and control cells were kindly donated by Michael Malim (37); CYPA knockdown and control U87-MG cells were cultured under 1 μg puromycin. Human macrophages were isolated from whole blood, obtained from the university hospital of Heinrich Heine University Düsseldorf (ethical approval study number 3180). Macrophages were maintained in RPMI 1640 containing 1,000 U/ml monocyte colony-stimulating factor (M-CSF).

Plasmids. The replication-competent HIV-1 N DJO0131, HIV-1 O RBF206, HIV-1 P RBF168, SIVcpzPtt MB897 clones were kindly provided by Frank Kirchhoff. SIVgorCP2139, and SIVcpzPts clone TAN1.910 clones were obtained from NIH AIDS repository (38). The murine leukemia virus (MLV) packaging construct pHIT60, which encodes the *gag-pol* of Moloney MLV was provided by Jonathan Stoye (39). Reporter viruses for HIV-1 N, HIV-1 O, HIV-1 P, and SIVgor were constructed as follow: Using fusion PCR, *nanoluciferase* gene was cloned in replacement of *nef* of HIV-1 N, HIV-1 O, HIV-1 P, and SIVgor. Two stop codons were introduced in the envelope genes of these viruses, as VSV-G was to be used for envelope. Capsid mutant reporter viruses of HIV-1 M, HIV-1 N, HIV-1 O and HIV-1 P were generated with fusion PCR using specific primers

including those with desired mutations. HIV-1 M with HIV-1 N or HIV-1 O or HIV-1 P capsid were made by fusion PCR, their inserts were cloned in PmlI-MfeI digested pMDLg/pRRE vector to produce chimeric gag-pol of HIV-1 M with CA genes of other viruses: pMDLg/pRRE.HIV-1 N CA, pMDLg/pRRE.HIV-1 O CA, pMDLg/pRRE.HIV-1 P CA. Complete gag-pol constructs for HIV-1 N, HIV-1 O, and HIV-1 P were constructed using the HIV-1 M pMDLg/pRRE plasmid and replacing HIV-1 M gag-pol by digestion with PmlI and BspEI and insertion of gag-pols of interest, produced through a series of overlapping PCR reactions, to make pMDLg/pRRE.HIV-1 N, pMDLg/pRRE.HIV-1 O, pMDLg/pRRE.HIV-1 P and pMDLg/pRRE.SIVgor. CYPA binding loop capsid mutants were made through PCR with primers bearing specific CYPA binding loops sequences and their inserts were respectively cloned in specific vectors to make HIV-1 M.N loop, HIV-1 M.O loop, and HIV-1 N.M loop. HIV-1 vector pSIN.PPT.CMV.Luc.IRES.GFP expresses firefly luciferase and GFP. psPAX2 was obtained from the NIH AIDS Reagent Program (Cat# 11348); pRSV-Rev, pMDLg/pRRE and pMD.G (VSV-G) have been described (40). Using fusion PCR on TRIMCyp in pLNCX2 plasmid (41), fusion PCR was used to introduce the desired mutations in the CYPA domain; N66D, H69R or N66D-H69R rhTRIMCyp-HA mutants were generated.

Transfection and viral particle production. The pMDLg/pRRE based viral particles production was done using: pMDLg/pRRE (800 ng), pSIN.PPT.CMV.Luc.IRES.GFP (800 ng), pRSV-Rev (400 ng), and pMDG.VSV-G (200 ng). For nanoluciferase-based reporter viruses (HIV-1 N, O, P, SIVgor, SIVcpz), 10⁶ HEK293T cells were seeded, the following day, these cells were transfected using 200 ng VSV-G and 2000 ng of viral plasmids using polyjet (Tebubio GmbH, Offenbach, Germany). 48 hrs post-transfection, viral particles were collected. Where needed, the reverse transcriptase (RT) activity of viruses was quantified using the previously described approach (42).

Generation of stable cells expressing TRIM5 proteins. Viral particles produced in HEK293T cells using a pLNCX2.TRIMCyp construct, pHIT60, and pMD.G (VSV-G) were used to transduce CrFK cells for three days, followed by a selection under 400 μ g/ml G418 (Biochrom GmbH, Berlin, Germany), for the expression of HA-tagged wild type and mutant rhTRIMCyp proteins. Protein expression was confirmed with immunoblots. Cells expressing empty pLNCX2 vector were used for control.

Single round infection assay. 10 x 10⁴ CrFK cells or 5 x 10³ (U-87 MG) cells were seeded into 96-well plates and infection was performed the following day. For experiments involving cyclosporin A (CsA, Sigma Aldrich, Germany), 1 to 10 μM of CsA or control DMSO were used to treat cells 2 hrs before infection. Cells were then infected with different reporter viral particles and after 48 to 72 hrs, luciferase activity was measured. For infection with nanoluciferase-containing reporter viruses, cells were washed with phosphate-buffered saline (PBS) three times before lysis and luciferase measurement, in addition to medium change 24 hrs following infection, to eliminate the effect of background nanoluciferase. Nanoluciferase activity was measured with Nano-Glo Luciferase system (Promega, Mannheim, Germany) and firefly luciferase activity was measured with the Steady-Glo Luciferase system (Promega) on a MicroLumat Plus luminometer (Berthold Detection Systems, Pforzheim, Germany). Each experiment was performed in triplicates for at least three times.

Pulldown assays and immunoblots. The GST-CYPA based pulldown experiments followed a protocol previously described (43). To confirm the expression of primate TRIM5 proteins, cells were lysed using RIPA lysis buffer (25 mM Tris-HCl [pH 8.0], 137 mM NaCl, 1% NP-

40, 1% glycerol, 0.5% sodium deoxycholate, 0.1% sodium dodecyl sulfate (SDS), 2 mM EDTA, and protease inhibitor cocktail set III (Calbiochem, Darmstadt, Germany). The cell lysate was centrifuged at 14,800 rpm for 20 min at 4°C. The protein supernatant was denatured using Roti-load sample buffer (Roth, Karlsruhe, Germany) and was used for SDS PAGE. Mouse primary anti-HA (MMS-101P, Covance, Münster, Germany, 1:7.500 dilution) for HA-tagged proteins, anti-human TRIM5α (rabbit monoclonal, # 143265; Cell Signaling Technology Europe BV, Frankfurt, Germany), anti-CYPA (mouse monoclonal; Santa Cruz Biotechnology) (1:500 dilution), CYPA.GST was detected using mouse anti-GST (SAB4200237-200UL, Sigma-Aldrich, Germany,1:7500 dilution)) were used. For viral proteins, viral supernatant was centrifuged through 20% sucrose gradient for a minimum of 4 hrs at 4°C, 14.800 rpm. The supernatant was discarded, and the viral pellet was lysed using RIPA buffer for 5 min followed by denaturation at 95°C in Roti-load sample buffer for 5 min and SDS PAGE using anti-p24 antibody (NIH).

Modeling of HIV-1 capsid variants. The structural model of the HIV-1 M capsid and CYPA generated by TopModel (44, 45) taken from (43). The capsid-CYPA complex was formed by superimposing the structures of the components onto the proteins of the cryo-EM structure PDB ID 5FJB. Mutations at the CYPA binding loop to HIV-1 N, HIV-1 O, and the HIV-1 M A88V, M91L, and H87P variants were introduced with SCWRL (46). HIV-1 N P87H and I91L monomers were modeled with (47). The capsid-CYPA complex was formed as above. PDB2PQR (48) was used to determine the protonation state at pH = 7.4 with the help of PROPKA 3 (49). The systems were packed using PACKMOL-Memgen (46) adding KCl in a concentration of 0.15 M and using a minimum distance between the protein(s) and the edges of the water box of 15.0 Å. The ff19SB force field (44) was used for the proteins, the OPC force field (50) with the corresponding Li/Merz ion parameters (49) was used for water and ions, respectively.

Thermalization, density adjustment, and dihedral modification for PMF calculations.

Thermalization and density adjustment were carried out using pmemd from the Amber22 software package (51, 52) with a time step of 2 fs. The Langevin thermostat (53) and Berendsen barostat (44) were used for temperature and pressure control, respectively. For the treatment of long-range electrostatic interactions, the Particle Mesh Ewald method (54) was used with a direct-space non-bonded cutoff of 9.0 Å. The SHAKE algorithm was used to constrain bond lengths involving hydrogen atoms (55). For each loop variant (HIV-1 M, HIV-1 N, HIV-1 O, HIV-1 M A88V), the loop either binding to CYPA or unbound was turned at the ω dihedral between G89 and P90 in 3° steps, which leads to 121 windows for each setup. The dihedral was modified to the target value during 10.000 steps of relaxing the system with the steepest decent algorithm followed by 10.000 steps with the conjugate gradient algorithm applying a force at the ω dihedral of 200 kcal mol⁻¹ rad⁻². During 10 ns, the system was heated to 300 K and 1 bar under NPT conditions.

Umbrella sampling and PMF calculations. For each window, 20 ns of umbrella sampling simulations in the NPT ensemble were performed, using a harmonic restraining potential with a force constant of 200 kcal -mol⁻¹ rad⁻² and writing out the ω dihedral every 50 simulation steps. The ω dihedral distribution was analyzed with the Weighted Histogram Analysis Method (WHAM) v2.0.9.1 (48). The periodicity was considered in the analysis, histogram limits were set to -0.5° and 360.5° for 722 bins in total, and the tolerance was set to 10^{-7} kcal

- mol⁻¹. The histograms showed a median overlap of 25% between contiguous windows 229
- 230 (Figures S4 –S11, Table S1), well suited for PMF calculations (56).
- 231 The error along the PMF (G(x)) was estimated by block averaging; for each system, the data
- 232 were separated into five parts of 4 ns each. The squared error in the estimate of the mean
- 233 position of ω in window i (var($\overline{x_i}$)) was calculated based on the block averages (for further
- 234 details see SI and eq. S1) (57). From there, the error was propagated to derive the variance of
- 235 PMFs (var[G(x)]) taking into account var($\overline{x_i}$) as well as the used force constant (k), the
- 236 sampling step size $(\Delta \omega)$, and the starting position (ω_0) as suggested by Zhu and Hummer (eq.
- 237 1) (54).

$$var[G(\mathbf{x})] \approx (k\Delta)^2 \sum_{i=1}^{\frac{(\mathbf{x}-\omega_0)}{\Delta}} var(\bar{\mathbf{x}}_i)$$
 eq. 1

- From var[G(x)], the standard deviation and the standard error of the mean were computed. 238
- 239 For error propagation when subtracting values of windows n and m, e.g., for obtaining
- $\Delta G^{\#}_{t \to c}$, SEM was calculated according to eq. 2: 240

$$SEM = \sqrt{SEM_m^2 + SEM_n^2}$$
 eq. 2

- 241 Individual states, e.g., cis ($\omega = 0^{\circ}$), trans ($\omega = 180^{\circ}$), and transition state ($\omega = 90^{\circ}$), were
- 242 visually checked, and figures were prepared with PyMOL.

243 244 245

246

Results

Construction of non-M HIV and SIVgor reporter viruses.

- 247 We constructed novel nanoluciferase-based reporter viruses for HIV-1 N, HIV-1 O, HIV-1 P,
- 248 and SIVgor. Nanoluciferase was cloned in replacement of nef genes. In addition, two stop
- 249 codons were inserted in the *env* genes. Production of VSV-G-pseudotyped viral particles was
- 250 done through transfection of HEK293T cells, and such virions were tested on human HeLa
- 251 cells, for infectivity by nanoluciferase measurement, two days after infection (data not
- 252 shown). We also constructed pMDLg/pRRE-based gag-pol constructs for HIV-1 N, HIV-1
- 253 O, HIV-1 P and SIVgor. Such constructs were made by replacing HIV-1 M gag-pol in
- 254 pMDLg/pRRE with non-M or SIVgor gag-pol.

255 256

Non-M HIVs are inhibited by human TRIM5α in human cells.

- 257 To test whether the replication of non-pandemic HIVs is restricted by human TRIM5 α , equal
- 258 amounts of reporter viruses of non-M HIVs (HIV-1 N, HIV-1 O, HIV-1 P) and SIVs
- 259 (SIVcpzPtt, SIVcpzPts, SIVgor) were used for infections of human wildtype (WT) U-87 MG
- 260 and huTRIM5α knockout (KO) U-87 MG cells (37) (Fig. 1A). In addition, we included
- 261 reporter viruses for HIV-1 M and for the equine infectious anemia infectious virus (EIAV);
- 262
- EIAV is known to be sensitive to human TRIM5α (19). While the infectivity of HIV-1 M 263 was equal in WT and TRIM5 KO cells, infection by non-M HIVs but also SIVgor was
- 264 enhanced when huTRIM5α was knocked down (Fig. 1B, Fig. S1A). Infection by HIV-1 N
- 265 increased to up to three folds in the huTRIM5α KO cells as compared to control cells,
- 266 infection by HIV-1 O, HIV-1 P, and SIVgor reached 2.5-, 3.5-, and 2-folds, respectively in 267 the absence of huTRIM5α, suggesting inhibition of these viruses by human TRIM5α. EIAV
- 268 showed 6.5-fold higher infectivity in the absence of huTRIM5α, compared to WT cells. In
- 269 contrast, SIVcpzPtt and SIVcpzPts did not benefit from the absence of huTRIM5a (Fig. 1B),

as described before (58). We also compared infection of WT U-87 MG cells with HIV-1 M vs. non-M HIV-1s virions produced by their respective *gag-pol* expression plasmids and confirmed a strongly reduced infectivity of HIV-1 N, O and P compared to the infectivity of HIV-1 M (Fig. S1B). The restriction of non-pandemic HIV-1s was seen over a wide range of virus input in WT U87-MG cells and in primary human macrophages (Fig. S2).

Capsid and its CYPA binding loop mediate differences in sensitivity to huTRIM5a.

Since TRIM5 α is a capsid-binding factor (11), we opted to investigate on the mechanisms behind differences in sensitivity to huTRIM5 α between HIV-1 M and non-pandemic HIVs. We transferred the capsid encoding sequence from HIV-1 N, HIV-1 O, HIV-1 P, to HIV-1 M in the *gag-pol* expression construct pMDLg/pRRE representing HIV-1 M sequence (Fig. 1C). In contrast to WT HIV-1 M, chimeric viruses with capsid from non-M viruses were inhibited 2.5-8-fold in WT cells compared to huTRIM5 α KO cells (Fig. 1D), confirming the role of viral capsid for restriction by human TRIM5 α .

Reports have described that in human cells the capsid-interacting cellular protein cyclophilin A (CYPA) protects HIV-1 M against the antiviral activity of huTRIM5α (20, 21). In capsid, CYPA binds to a loop between helix 4 and helix 5, termed CYPA binding loop. Here CYPA directly interacts with residues G89 and P90 (23), which are conserved in pandemic and non-pandemic HIVs. However, other residues between these viruses show variations, HIV-1 N, and HIV-1 P share an identical CYPA binding loop (Fig. 1E, Fig. S3). To explore the impact of loop variability, we swapped in capsid the CYPA binding loops between HIV-1 M, HIV-1 N, and HIV-0. Thus, we created HIV-1 M gag-pol constructs with a CYPA binding loop of HIV-1 N (identical to HIV-1 P) or HIV-1 O. In reverse, we transferred the HIV-1 M CYPA binding loop to HIV-1 N or HIV-1 O gag-pol constructs. Stunningly, viruses that had the CYPA binding loop of non-pandemic HIVs showed a restriction in WT cells compared to TRIM5α KO cells, and non-pandemic viruses with a CYPA binding loop of HIV-1 M escaped the restriction by TRIM5α (Fig. 1F). These findings demonstrated that the capsid CYPA binding loops account for differences in infection levels of pandemic and non-pandemic HIVs in huTRIM5α expressing cells.

Capsid residue at position 88 mediates HIV sensitivity to huTRIM5α.

In the capsid CYPA binding loop, the human CYPA protein binds strongly to residues G89 and P90 (23) but also A88 binds in the active site groove of CYPA (59). We hypothesized that variability in residue 88 in the CYPA binding loops could explain our observations regarding the differential sensitivity of HIV-1 M and the non-pandemic HIV-1s to TRIM5α. We infected both WT and TRIM5α KO cells with reporter viruses that had mutations in the CYPA binding loop at position 88, HIV-1 M A88V, HIV-1 N V88A, HIV-1 O M88A or HIV-1 P V88A, and compared their infectivity to the corresponding WT viruses. For HIV-1 M, we included the well-characterized HIV-1 M G89V and A88V-G89V capsid mutants, which do not bind CYPA. As expected, both mutations in HIV-1 M, A88V and G89V were strongly inhibited in WT U-87 MG cells compared to WT virus (Fig. 2A). However, in TRIM5α KO cells infections by both capsid mutants were not reduced compared to WT HIV-1 M, with infection by the A88V mutant even 4.3-fold higher than infection by WT virus (Fig. 2B, Fig. S4A, B). Infections by capsid mutants of non-pandemic HIVs showed a contrasting pattern. In WT cells, the infectivity of HIV-1 N V88A was 5-fold higher, of HIV-1 O M88A was 2.3 folds higher, and of HIV-1 P V88A was 2.1 folds higher than infections by their WT viruses (Fig. 2C). However, these capsid mutants of non-pandemic viruses had a similar infectivity to WT virus in TRIM5a KO cells (Fig. 2D). To further analyze if other residues in the CYPA binding loop could inhibit the protection in HIV-1 M or induce a

- 320 resistance to TRIM5α in HIV-1 N, additional mutations were tested (Fig. S5). As a positive 321 control, we included the A92E change in HIV-1 M and the P92E mutation in HIV-1 N. As it 322 was shown that the Ala 92 to Glu mutation disrupts the binding of human TRIM5α to HIV-1 323 M viral cores (20). In HIV-1 M, the mutations H87P, I91L, and A92E, in contrast to A88V or
- 324 G89V did not enhance the sensitivity to TRIM5α (Fig S5A). In HIV-1 N, however, the
- 325 reverse mutations P87H, L91I, or P92E, similar to V88A induced a protection against
- 326 TRIM5α (Fig. S5B). Together, these findings show that residue 88 in the CYPA binding loop
- 327 of capsid is a unique determinant of TRIM5α restriction in pandemic and non-pandemic
- 328 HIV-1. Other CYPA loop residues in non-pandemic HIV-1 may be additionally important.

329 330

Pandemic and non-pandemic HIV-1 capsids bind CYPA.

331 With the observed differences in capsid CYPA loop between M and non-M HIV-1s (Fig. 1F), 332 we wanted to test whether all four viruses interact with CYPA similarly. Using a GST-tagged 333 CYPA, we assessed CYPA-capsid interaction in pulldown experiments. Immunoblots of 334 these precipitations found similar levels of capsid protein for all four HIV-1s (Fig. 2E). In 335 addition, we found that CYPA is packaged in virions of pandemic and non-pandemic HIV-1s 336 (Fig. 2F). To understand if these viruses package similarly CYPA, we exposed them to 337 increasing amounts of cyclosporine A (CsA), a drug that binds CYPA and prevents CYPA 338 interaction with capsid. The dose-dependent reduction of CYPA packaging showed a small 339 difference between HIV-1 M and the non-pandemic HIV-1s. A CsA dose of 1 μM reduced

340 virion-associated CYPA by around 70% in the context of non-M HIVs, as opposed to only 341 40% by HIV-1 M, possibly suggesting differences in CYPA binding strength between

342 capsids of these viruses (Figs. 2F, G).

343 344

345

Cyclophilin A decreases the isomerization barrier the most for HIV-1 M wild type and variants that are protected against TRIM5α.

- 346 To address the question if the binding of CYPA to HIV-1 capsid has different effects between 347
- the pandemic HIV-1 M versus HIV-1 N, HIV-1 O, HIV-1 P, or variants of HIV-1 types, we 348 performed potential of mean-force (PMF) computations of the isomerization reaction
- 349 catalyzed by CYPA. HIV-1 P was not considered because the loop composition is as in HIV-
- 350 1 N. The isomerization occurs between the *trans* and *cis* conformations of the peptide bond
- 351 formed by residues G89 and P90 in the CYPA binding loop of the capsid (36). The
- 352 conformational change is characterized by the torsion angle ω (trans: $\omega = 180^{\circ}$, cis: $\omega = 0^{\circ}$;
- 353 Figs. 3A, B). The PMF is the free energy change during the isomerization evaluated along the
- 354 reaction coordinate ω (Fig. 3C); the PMF describes an average over the conformations of the
- 355 surrounding protein residues and solvent molecules, such that the effect of other CYPA
- 356 binding loop residues that vary among different HIV-1 clades is considered.
- 357 We computed PMFs of the isomerization in the presence and absence of CYPA and
- 358 calculated the free energy difference $\Delta G_{\rm t,c}$ as the difference between the PMF values for the trans and cis conformations (Fig. S5, Table S2, Fig. 3D) as well as the barrier height $\Delta G_{t_{\Delta}c}^{\#}$ 359
- 360 as the difference between the PMF values for the trans conformation and the maximal value
- 361 at $\omega \approx 90^{\circ}$ (Fig. S5, Table S3, Fig. 3D).
- In the absence of CYPA, $\Delta G_{\rm t,c} \approx 1.7$ to 2.3 kcal mol⁻¹ for the WT systems (Fig. S6, Table 362
- 363 S2), indicating that the trans conformation of the peptide bond between residues G89 and
- 364 P90 is preferred over the *cis* conformation by \sim 95 : 5 in line with NMR experiments (36).
- 365 This indicates that the energetic description of the states at the minima is appropriate,
- 366 confirming previous work (60).

- In the presence of CYPA, the barrier height $\Delta G^{\dagger}_{t,c}$ decreases in all WT systems by 1.7 2.9 367
- kcal mol⁻¹ compared to the absence of CYPA (Fig. 3D, Fig. S6, Table S3), indicating a faster 368
- isomerization when catalyzed by CYPA, as expected. The decrease of $\Delta G_{t_{\Delta}c}^{\#}$ is the largest 369
- 370 for HIV-1 M, indicating that the isomerization is most accelerated by CYPA for HIV-1 M,
- 371 which is protected against TRIM5α (Fig. 1), and that it is ~5-10 fold faster for HIV-1 M than
- 372 for the other WT systems, which are not protected (Fig. 1).
- 373 As to variants, HIV-1 M A88V is not protected, and its behavior differs from the WT in the
- 374 presence of CYPA: The trans conformation is more favorable, and the isomerization barrier
- 375 is comparable to that in solution (Fig. S6, Tables S2 and S3). This may be caused by V88
- 376 sticking into the hydrophobic surface of CYPA, which hampers the isomerization (Fig. S7).
- 377 Notably, variants HIV-1 N L91I and P87H, which become protected against TRIM5α in
- contrast to the WT (Fig. S5B), show decreases in $\Delta G_{t_{\Delta}c}^{\#}$ in the presence of CYPA that are as 378
- 379
- large as or comparable to that in HIV-1 M. The reverse mutation in HIV-1 M, I91L, keeps the variant protected (Fig. S5A) and, analogously, the decrease in $\Delta G^{\#}_{t \to c}$ is the fourth largest. 380
- Overall, the magnitude of the decrease in $\Delta G^{\#}_{t \to c}$ in the presence of CYPA allows for an 381
- almost perfect ordering of the investigated HIV-1 types and variants, with protected ones 382
- 383 showing generally the largest decreases (Fig. 3D). The change in $\Delta G_{t,c}$ would not allow such
- 384 an ordering. Although the quantitative relation of barrier heights derived from PMFs to
- 385 kinetics requires caution (61), this finding suggests that the kinetics of the trans/cis
- 386 isomerization plays a decisive role in the protective effect of CYPA for HIV-1 M.

Rhesus TRIMCyp inhibits non-M HIVs.

387 388

389

390

391

392

393

394

395

396

397

398

399

400

401

402

403

404

405

406

407

408

409

410

411

412

413

414

TRIMCyp proteins differentially halt retroviral infection through the binding of their CYPA domain to capsid CYPA binding loop, early during infection, this inhibition can be blocked by cell treatment with CsA (26). For instance, owl monkey TRIMCyp is active against HIV-1 but not HIV-2 and rhTRIMCyp from rhesus macaques (rh) inhibits HIV-2 but not HIV-1 M (18, 41). In rhTRIMCyp, CYPA differs from human CYPA by two residues, the CYPA in rhTRIMCyp has N66 and H69 while human CYPA has D66 and R69 (62). It was shown that HIV-1 M's resistance and HIV-1 O's inhibition by rhTRIMCyp were due to the presence of N66 and H69 in this CYPA domain (59). To further understand if rhTRIMCyp or a variant in which we reversed the two residues to D66 and R69 have differential antiviral activity to pandemic and non-pandemic HIV-1, we generated cell lines expressing WT rhTRIMCyp or its CYPA mutants N66D, H69R, N66D-H69H (Fig. 4A). We challenged such cells with HIV-1 M, HIV-1 N, HIV-1 O, HIV-1 P and SIVgor. As expected, rhTRIMCyp did not reduce the infectivity of HIV-1 M, but strongly inhibited HIV-1 O (58). In addition, all other viruses, HIV-1 N, HIV-1 P, SIVgor were also strongly inhibited in cells expressing rhTRIMCyp by or more than 90% (Figs. 4B, C and Fig. S8). TRIMCyp with a human identical CYPA domain (N66D H69R, DR), recognized pandemic and non-pandemic viruses and displayed strong antiviral activity, further indicating that human CYPA interacts with all tested viruses. Mutating only residue H69R (NR) in rhTRIMCyp caused a complete loss of antiviral activity against HIV-1 N and HIV-1 O, in addition to remaining inactive against HIV-1 M. However, HIV-1 P and SIVgor were still inhibited by around 50%. In contrast, mutating N66 to the human D in rhTRIMCyp (DH mutant), generated an antiviral protein that inhibited efficiently all viruses (Figs. 4B, C and Fig. S8). Previous data suggested that capsid residue 88 in the CYPA binding loop mediates differential interaction of HIV-1 M and O with rhTRIMCyp (59). The mutations in residue 88 reversed the resistance of HIV-1 M and the sensitivity of HIV-1 N, HIV-1 O and HIV-1 P to rhTRIMCyp (Figs. 4B, C). The non-pandemic HIVs with capsid mutations at position 88 were still sensitive to antiviral activity of TRIMCyp.DR, as

was HIV-1 M A88V (Fig. 4B). The HIV-1 M G89V, was predictably not inhibited by any TRIMCyp protein, likely because the G89V mutation prevented the interaction of TRIMCyp (Fig. 4B). These data suggest that the human CYPA domain in TRIMCyp proteins and likely free CYPA can recognize the incoming viral cores of non-pandemic HIV-1s.

419 420

421

422

423

424

425

426

427

428

429

430

431

432

433

434

435

436

437

438

439

440

441

442

443

444

445

446

Pandemic and non-pandemic HIVs show different dependencies on CYPA.

To test whether the depletion of CYPA affects pandemic and non-pandemic HIVs differently, a CYPA knockdown in U-87 MG cells and huTRIM5α KO U-87 MG using the CRISPR/Cas9 system was done (Fig. 5A). CYPA knockdown in WT cells was associated with a strong and significant inhibition of HIV-1 M infectivity by up to 86%, and while the TRIM5α KO generated infections comparable to WT cells, the cells that lost TRIM5α and additionally CYPA expression were unexpectedly less infectable than WT or TRIM5α KO cells, suggesting that CYPA function for HIV-1 M is beyond protection against TRIM5α (Fig. 5B). Non-M HIVs and SIVgor were also tested in such conditions. The CYPA KD affected the non-pandemic HIVs less than HIV-1 M and caused only 50% inhibition. In further contrast to HIV-1 M, cells with no TRIM5α and no CYPA were much better infectable than the TRIM5α KO cells by the non-pandemic HIV-1s (Figs. 5C, E). Infection with SIVgor differed from all HIV-1s and was not affected by CYPA KD in WT or TRIM5α KO cells, demonstrating that the CYPA KD did not impair cell vitality (Fig. S9A). In an additional approach, we tested CsA treatment of cells in infection experiments. Increasing levels of CsA (0.1 µM to 10 µM) inhibited up to 91% of infection by HIV-1 M in WT U87 MG cells (Fig. 5F). In WT cells treated with 1 µM CsA, HIV-1 N was inhibited by 41%, HIV-1 O by 57%, HIV-1 P by 66%, while HIV-1 M's infectivity was decreased by 74%. Interestingly, high CsA concentrations had no further effect on infections by HIV-1 N and HIV-1 O but inhibited 77% of HIV-1 P (Fig. 5F). As expected, SIVgor did not react to CsA treatment of WT U-87 MG cells (Fig. S9B). Predictable, in CYPA-depleted cells, CsA treatment lost almost all its antiviral activity and only HIV-1 M showed some mild inhibition using 10 μM CsA (Fig. 5G). In TRIM5α KO cells, CsA treatment inhibited only HIV-1 M but had no effect on non-M HIVs, mirroring data obtained with CYPA KD (Fig. 5H). In CYPA and TRIM5α double depleted cells, CsA had no significant inhibitory activity against any virus tested, suggesting that CsA itself does inhibit these viruses (Fig. 5I, Fig. S9B). Together, these data suggest that the non-pandemic HIV-1s have a weak and partial

447 448 449

450

451

452

453

454

455

456

457

458

459

460

461

462

463

464

Discussion

protection against TRIM5α by its CYPA binding.

The reason(s) why non-M HIVs did not extensively spread in the human population remain(s) elusive. Some reports have pointed out differences in GAG capsid sequences but also differences in the functional activity of viral accessory proteins (63, 64). Here, we found that non-pandemic HIV-1 are subject to restriction by human TRIM5 α . While it was shown that CYPA forms a protective layer around the viral core of HIV-1 M to prevent destruction by human TRIM5 α (20, 21), the CYPA interaction with non-pandemic HIV-1 N, O and P does not protect strongly against TRIM5 α .

Our data demonstrate that the non-pandemic HIV-1s interact with and bind CYPA to a level that appears similar to the level of binding of HIV-1 M. Surprisingly, our findings show that the viral capsid CYPA binding loop determines the different sensitivities to TRIM5α of HIV-1 M and the non-pandemic HIV-1s. A recent report (65) has suggested capsid residues, such as residue at position 50, as important for differential sensitivity to TRIM5α by HIVs. Our findings suggest that more than one region of the capsid is involved in the regulation of TRIM5α activity. Thus, we postulate that not the binding of CYPA itself, but the nature of

CYPA capsid interaction is a regulator of TRIM5α sensitivity. Despite an identical GP motif in capsid CYPA binding loops in pandemic and non-pandemic HIV-1s, these viruses engage CYPA differently, suggesting an important role from other residues of the CYPA binding loop.

Moreover, a rescue of infection of non M HIV-1s, when their capsids were specifically mutated at position 88 or when the CYPA domain of rhTRIMCyp was mutated at position 66 or 69, shows the importance of the capsid CYPA binding loop for such restriction by rhTRIMCyp, as previously shown for HIV-1 M, HIV-1 O, and HIV-2 (18, 59). It is possible that the presence of valine (HIV-1 N and HIV-1 P capsid) or methionine for HIV-1 O at position 88 of the capsid, as opposed to alanine in the HIV-1 M, changes capsid conformation and allows availability of the loop to other host factors like TRIM5α, in addition to CYPA binding. This may restrict non-M HIVs by TRIM5α, but this hypothesis will need clarification.

Based on our study results, we postulated that the CYPA trans/cis isomerization activity on the capsid G89-P90 peptide bond (36, 61) differs between HIV-1 M and non-pandemic HIVs and that this difference changes the binding strength of TRIM5α in an unknown way that may involve allostery (35). This hypothesis is supported by the PMF computations of the isomerization reaction. The capsid binding sites for TRIM5α are still ill-defined, although it is known that the binding involves the capsid CYPA binding loop (13). In crystal structures, the loop of HIV-1 M is in the *trans* conformation in the presence of CYPA, whereas the loop in HIV-1 O is in the cis conformation in the presence of CYPA (61). It is not known which of the conformations is preferred under native conditions. However, TRIM5α should bind neither too strongly nor too weakly to the HIV-1 capsid to build an antiviral scaffold around the core (66). Considering that in G-P peptides the trans conformation prevails according to crystal structure (67) and NMR spectroscopy (68) analyses, our results lead us to speculate that a faster isomerization process might lead to reaching a higher proportion of cis conformation faster in the CYPA binding loop, which might affect TRIM5α binding. This would be most relevant for HIV-1 M. In turn, and, in line with this, in the HIV-1 M A88V capsid mutant in the presence of CYPA, the isomerization barrier remains unchanged and almost as high as in the other HIV-1 WT in solution, which might explain why this variant does not show resistance against TRIM5α anymore. This would also explain why non-M HIV-1s with valine or methionine are also inhibited by TRIM5 α . The magnitude of the decrease in the isomerization barrier in the presence of CYPA allows for an almost perfect ordering of all HIV-1 types and variants investigated in PMF computations, with protected ones showing generally the largest decreases, suggesting that the kinetics of the trans/cis isomerization plays a decisive role in the protective effect of CYPA for HIV-1 M.

The non-pandemic HIV-1s likely face several restrictions in human cells that slow a rapid adaptation. Ala88 is conserved in different HIV-1 M isolates, and Val in the few cases of HIV-1 N and HIV-1 P. However, HIV-1 O isolates show more variability and there are viruses that have at position 88 Val, Met, or Ile (Fig. S3). SIVgor, the ancestor virus of HIV-1 O and HIV-1 P has also Val at position 88 and shows similar restriction by human TRIM5α (Fig. S1). SIVcpz is escaping human TRIM5α likely by its A88. Therefore, the generation of HIV-1 M was not restricted by human TRIM5α. It is, however, puzzling to understand why in the generation of HIV-1 N the A88 changed to V88. As we show in Figs. 2B and S4, HIV-1 M with an A88V mutation has higher infectivity in cells lacking TRIM5α compared to WT virus. Thus, HIV-1 N may have evolved in an environment with reduced antiviral TRIM5α activity.

515516

517

ACKNOWLEDGEMENTS

- We thank Wioletta Hörschken, Björn Wefers, and Yvonne Dickschen for excellent technical
- assistance. We thank Thomas Gramberg, Beatrice H. Hahn, Frank Kirchhoff, Michael Malim,
- 520 Daniel Sauter, Heiner Schaal, Jonathan P. Stoye, Greg Towers, and Stephen R. Yant for
- 521 reagents. The following reagents were obtained through the NIH AIDS Research and
- 522 Reference Reagent Program, Division of AIDS, NIAID, NIH: psPAX2 (Cat# 11348) from
- 523 Didier Trono, SIVcpz TAN1.910 infectious molecular clone (Cat #11496) and
- 524 SIVgorCP2139 (Cat # ARP-11722) from Jun Takehisa, Matthias H. Kraus and Beatrice H.
- 525 Hahn. APT is supported by German Academic Exchange Service (DAAD), SL is supported
- 526 by Chinese Government Scholarship, CM is supported by the Heinz-Ansmann foundation for
- 527 AIDS research. This work was, in part, supported by Deutsche Forschungsgemeinschaft
- 528 (DFG) through GRK 2158/2 (project number 270650915) to HG. HG is grateful for
- 529 computational support and infrastructure provided by the "Zentrum für Informations- und
- 530 Medientechnologie" (ZIM) at the Heinrich-Heine-University Düsseldorf and the computing
- 531 time provided by the John von Neumann Institute for Computing (NIC) to HG on the
- supercomputer JUWELS at Jülich Supercomputing Centre (JSC) (user ID: VSK33).

533 534

535

References

- 536 1. P. M. Sharp, B. H. Hahn, Origins of HIV and the AIDS Pandemic. *Cold Spring Harb* 537 *Perspect Med* **1**, a006841 (2011).
- 538 2. S. Bush, D. M. Tebit, HIV-1 group O origin, evolution, pathogenesis, and treatment: Unraveling the complexity of an outlier 25 years later. *AIDS Rev* 17, 147–158 (2015).
- 540 3. S. M. Bell, T. Bedford, Modern-day SIV viral diversity generated by extensive recombination and cross-species transmission. *PLoS Pathog* **13**, e1006466 (2017).
- 542 4. A. P. Twizerimana, R. Scheck, D. Häussinger, C. Münk, Post-entry restriction factors of SIVcpz. *Future Virol* **13**, 727–745 (2018).
- 5. R. S. Harris, J. F. Hultquist, D. T. Evans, The Restriction Factors of Human Immunodeficiency Virus. *Journal of Biological Chemistry* **287**, 40875–40883 (2012).
- 546 6. M. H. Malim, P. D. Bieniasz, HIV Restriction Factors and Mechanisms of Evasion. 547 *Cold Spring Harb Perspect Med* **2**, a006940 (2012).
- 7. P. Staeheli, O. Haller, Human MX2/MxB: a Potent Interferon-Induced Postentry Inhibitor of Herpesviruses and HIV-1. *J Virol* **92** (2018).
- 550 8. G. Boso, C. A. Kozak, Retroviral Restriction Factors and Their Viral Targets: 551 Restriction Strategies and Evolutionary Adaptations. *Microorganisms* **8** (2020).
- 552 9. L. Cano-Ortiz, T. Luedde, C. Münk, HIV-1 restriction by SERINC5. *Med Microbiol Immunol* **212**, 133–140 (2023).
- 554 10. A. Reymond, *et al.*, The tripartite motif family identifies cell compartments. *EMBO J* **20**, 2140–51 (2001).
- 556 11. B. K. Ganser-Pornillos, O. Pornillos, Restriction of HIV-1 and other retroviruses by TRIM5. *Nat Rev Microbiol* **17**, 546–556 (2019).
- 558 12. S. B. Kutluay, D. Perez-Caballero, P. D. Bieniasz, Fates of Retroviral Core
- Components during Unrestricted and TRIM5-Restricted Infection. *PLoS Pathog* **9**, e1003214 (2013).
- H. Yang, et al., Structural insight into HIV-1 capsid recognition by rhesus TRIM5α.
 Proc Natl Acad Sci U S A 109, 18372–7 (2012).
- 563 14. T. Pertel, *et al.*, TRIM5 is an innate immune sensor for the retrovirus capsid lattice https://doi.org/10.1038/nature09976 (February 25, 2018).

- 565 15. D. M. Sayah, E. Sokolskaja, L. Berthoux, J. Luban, Cyclophilin A retrotransposition into TRIM5 explains owl monkey resistance to HIV-1. *Nature* **430**, 569–573 (2004).
- 567 16. G. Brennan, Y. Kozyrev, S.-L. Hu, TRIMCyp expression in Old World primates
- Macaca nemestrina and Macaca fascicularis. Proceedings of the National Academy of Sciences 105, 3569–3574 (2008).
- 570 17. S. Sebastian, J. Luban, TRIM5alpha selectively binds a restriction-sensitive retroviral capsid. *Retrovirology* **2**, 40 (2005).
- 572 18. E. E. Nakayama, T. Shioda, TRIM5α and species tropism of HIV/SIV. *Front Microbiol* **3**, 1–12 (2012).
- 574 19. D. T. Saenz, W. Teo, J. C. Olsen, E. M. Poeschla, Restriction of feline
- 575 immunodeficiency virus by Ref1, Lv1, and primate TRIM5alpha proteins. *J Virol* **79**, 15175–88 (2005).
- A. Selyutina, *et al.*, Cyclophilin A Prevents HIV-1 Restriction in Lymphocytes by
 Blocking Human TRIM5α Binding to the Viral Core. *Cell Rep* 30, 3766-3777.e6
 (2020).
- 580 21. K. Kim, et al., Cyclophilin A protects HIV-1 from restriction by human TRIM5α. Nat
 581 Microbiol 4, 2044–2051 (2019).
- 582 22. B. K. Ganser, S. Li, V. Y. Klishko, J. T. Finch, W. I. Sundquist, Assembly and Analysis of Conical Models for the HIV-1 Core. *Science* (1979) **283**, 80–83 (1999).
- 584 23. S. Yoo, *et al.*, Molecular recognition in the HIV-1 capsid/cyclophilin A complex. *J Mol Biol* **269**, 780–795 (1997).
- 586 24. M. E. C. Caines, *et al.*, Diverse HIV viruses are targeted by a conformationally dynamic antiviral. *Nat Struct Mol Biol* **19**, 411–416 (2012).
- 588 25. T. R. Gamble, *et al.*, Crystal structure of human cyclophilin A bound to the aminoterminal domain of HIV-1 capsid. *Cell* **87**, 1285–1294 (1996).
- 590 26. G. J. Towers, *et al.*, Cyclophilin A modulates the sensitivity of HIV-1 to host restriction factors. *Nat Med* **9**, 1138–1143 (2003).
- 592 27. E. Toccafondi, D. Lener, M. Negroni, HIV-1 Capsid Core: A Bullet to the Heart of the Target Cell. *Front Microbiol* **12**, 755 (2021).
- 594 28. N. A. Kootstra, C. Münk, N. Tonnu, N. R. Landau, I. M. Verma, Abrogation of postentry restriction of HIV-1-based lentiviral vector transduction in simian cells.
- 596 Proceedings of the National Academy of Sciences 100, 1298–1303 (2003).
- 597 29. E. K. Franke, H. E. H. Yuan, J. Luban, Specific incorporation of cyclophilin a into HIV-1 virions. *Nature* **372**, 359–362 (1994).
- 599 30. M. Thali, *et al.*, Functional association of cyclophilin A with HIV-1 virions. *Nature* 372, 363–365 (1994).
- W. Peng, *et al.*, Functional analysis of the secondary HIV-1 capsid binding site in the host protein cyclophilin A. *Retrovirology* **16**, 10 (2019).
- 32. Z. Ambrose, et al., Human immunodeficiency virus type 1 capsid mutation N74D
- alters cyclophilin A dependence and impairs macrophage infection. *J Virol* **86**, 4708–14 (2012).
- 505 J. Shi, J. Zhou, V. B. Shah, C. Aiken, K. Whitby, Small-molecule inhibition of human immunodeficiency virus type 1 infection by virus capsid destabilization. *J Virol* 85, 542–9 (2011).
- T. Schaller, *et al.*, HIV-1 capsid-cyclophilin interactions determine nuclear import pathway, integration targeting and replication efficiency. *PLoS Pathog* 7, e1002439 (2011).
- 612 35. M. Lu, et al., Dynamic allostery governs cyclophilin A–HIV capsid interplay.
- Proceedings of the National Academy of Sciences 112, 14617–14622 (2015).

- 614 36. D. A. Bosco, E. Z. Eisenmesser, S. Pochapsky, W. I. Sundquist, D. Kern, Catalysis of cis/trans isomerization in native HIV-1 capsid by human cyclophilin A. *Proceedings of the National Academy of Sciences* **99**, 5247–5252 (2002).
- J. M. Jimenez-Guardeño, L. Apolonia, G. Betancor, M. H. Malim, Immunoproteasome
 activation enables human TRIM5α restriction of HIV-1. *Nat Microbiol* 4, 933–940
 (2019).
- J. Takehisa, *et al.*, Generation of infectious molecular clones of simian immunodeficiency virus from fecal consensus sequences of wild chimpanzees. *J Virol* 81, 7463–75 (2007).
- 623 39. M. Bock, K. N. Bishop, G. Towers, J. P. Stoye, Use of a Transient Assay for Studying the Genetic Determinants of *Fv1* Restriction. *J Virol* **74**, 7422–7430 (2000).
- 40. T. Dull, *et al.*, A third-generation lentivirus vector with a conditional packaging system. *J Virol* **72**, 8463–71 (1998).
- 41. S. J. Wilson, *et al.*, Independent evolution of an antiviral TRIMCyp in rhesus macaques. *Proc Natl Acad Sci U S A* **105**, 3557–62 (2008).
- J. Vermeire, et al., Quantification of reverse transcriptase activity by real-time PCR as a fast and accurate method for titration of HIV, lenti- and retroviral vectors. PLoS One
 7, e50859 (2012).
- 43. A. P. Twizerimana, et al., Cell Type-Dependent Escape of Capsid Inhibitors by Simian
 Immunodeficiency Virus SIVcpz. J Virol 94 (2020).
- 634 44. P. Li, L. F. Song, K. M. Merz, Systematic Parameterization of Monovalent Ions 635 Employing the Nonbonded Model. *J Chem Theory Comput* **11**, 1645–1657 (2015).
- D. Mulnaes, et al., TopModel: Template-Based Protein Structure Prediction at Low
 Sequence Identity Using Top-Down Consensus and Deep Neural Networks. J Chem
 Theory Comput 16, 1953–1967 (2020).
- 639 46. G. G. Krivov, M. V Shapovalov, R. L. Dunbrack, Improved prediction of protein side-640 chain conformations with SCWRL4. *Proteins* 77, 778–95 (2009).
- 47. J. Jumper, *et al.*, Highly accurate protein structure prediction with AlphaFold. *Nature* 596, 583–589 (2021).
- 48. H. J. C. Berendsen, J. P. M. Postma, W. F. van Gunsteren, A. DiNola, J. R. Haak,
 Molecular dynamics with coupling to an external bath. *J Chem Phys* 81, 3684–3690 (1984).
- 49. M. H. M. Olsson, C. R. Søndergaard, M. Rostkowski, J. H. Jensen, PROPKA3:
 647 Consistent Treatment of Internal and Surface Residues in Empirical p K a Predictions.
 648 J Chem Theory Comput 7, 525–537 (2011).
- 50. S. Schott-Verdugo, H. Gohlke, PACKMOL-Memgen: A Simple-To-Use, Generalized
 Workflow for Membrane-Protein-Lipid-Bilayer System Building. *J Chem Inf Model* 59, 2522–2528 (2019).
- C. Tian, et al., ff19SB: Amino-Acid-Specific Protein Backbone Parameters Trained
 against Quantum Mechanics Energy Surfaces in Solution. J Chem Theory Comput 16,
 528–552 (2020).
- D. A. Case Ross C Walker UC San Diego, A. E. Thomas Cheatham, "Amber 2022
 Reference Manual Principal contributors to the current codes" (April 16, 2023).
- 53. S. Izadi, R. Anandakrishnan, A. V. Onufriev, Building Water Models: A Different Approach. *J Phys Chem Lett* **5**, 3863–3871 (2014).
- F. Zhu, G. Hummer, Convergence and error estimation in free energy calculations using the weighted histogram analysis method. *J Comput Chem* **33**, 453–465 (2012).
- 55. D. Quigley, M. I. J. Probert, Langevin dynamics in constant pressure extended systems. *J Chem Phys* **120**, 11432–11441 (2004).

- 56. J.-P. Ryckaert, G. Ciccotti, H. J. C. Berendsen, Numerical integration of the cartesian equations of motion of a system with constraints: molecular dynamics of n-alkanes. *J Comput Phys* **23**, 327–341 (1977).
- 666 57. A. Grossfield, "An implementation of WHAM: the Weighted Histogram Analysis Method Version 2.0.10" (March 9, 2023).
- 58. Z. Kratovac, *et al.*, Primate Lentivirus Capsid Sensitivity to TRIM5 Proteins. *J Virol* **82**, 6772–6777 (2008).
- 670 59. A. J. Price, *et al.*, Active site remodeling switches HIV specificity of antiretroviral TRIMCyp. *Nat Struct Mol Biol* **16**, 1036–1042 (2009).
- 672 60. U. Doshi, D. Hamelberg, Reoptimization of the AMBER Force Field Parameters for
 673 Peptide Bond (Omega) Torsions Using Accelerated Molecular Dynamics. *J Phys* 674 Chem B 113, 16590–16595 (2009).
- 675 61. B. R. Howard, F. F. Vajdos, S. Li, W. I. Sundquist, C. P. Hill, Structural insights into the catalytic mechanism of cyclophilin A. *Nat Struct Biol* **10**, 475–81 (2003).
- 677 62. C. A. Virgen, Z. Kratovac, P. D. Bieniasz, T. Hatziioannou, Independent genesis of chimeric TRIM5-cyclophilin proteins in two primate species. *Proc Natl Acad Sci U S A* **105**, 3563–8 (2008).
- 680 63. D. Sauter, *et al.*, Tetherin-driven adaptation of Vpu and Nef function and the evolution of pandemic and nonpandemic HIV-1 strains. *Cell Host Microbe* **6**, 409–21 (2009).
- 682 64. D. Sauter, F. Kirchhoff, Key Viral Adaptations Preceding the AIDS Pandemic. *Cell Host Microbe* **25**, 27–38 (2019).
- 684 65. L. Zuliani-Alvarez, *et al.*, Evasion of cGAS and TRIM5 defines pandemic HIV. *Nat Microbiol* 7, 1762–1776 (2022).
- 686 66. A. Yu, *et al.*, TRIM5α self-assembly and compartmentalization of the HIV-1 viral capsid. *Nat Commun* **11**, 1307 (2020).
- 688 67. A. T. Gres, *et al.*, X-ray crystal structures of native HIV-1 capsid protein reveal conformational variability. *Science* (1979) **349**, 99–103 (2015).
- 690 68. C. Tang, Y. Ndassa, M. F. Summers, Structure of the N-terminal 283-residue fragment of the immature HIV-1 Gag polyprotein. *Nat Struct Biol* **9**, 537–43 (2002).

Figure legends

693 694 695

- Fig. 1. TRIM5α depletion in human U-87 MG cells increases non-M HIVs infection in a
 capsid CYPA binding loop dependent way. (A) Immunoblot of WT and TRIM5α KO U-87
- MG cells. Anti-TRIM5 antibody was used to detect TRIM5α; anti-GAPH antibody was used
- to ensure equal protein loading. (B) WT or TRIM5α KO U-87 MG cells were infected with equal amounts of luciferase reporter viruses for HIV-1 M, HIV-1 N, HIV-1 O, HIV-1 P,
- 701 SIVcpzPtt, SIVcpzPts and EIAV. Two to three days later, luciferase activity was measured,
- 702 infection of KO cells was normalized to infection of WT cells. (C) HIV-1 N, HIV-1 O or
- 703 HIV-1 P capsids were cloned in HIV-1 M gag-pol as replacements for its WT capsid. (D)
- 704 HIV-1 M gag-pol with capsid of either HIV-1 N, O or P were tested in WT and TRIM5α KO
- 705 U-87 MG cells. Two to three days after infection, luciferase activity was measured; infection
- of KO cells was normalized to infection of WT cells. (E) Protein sequence alignment of CYPA binding loop (box) regions of capsids of HIV-1 M, N, O and P and HIV-2. (F) Using
- their respective *gag-pol* constructs, CYPA binding loop from HIV-1 N or HIV-1 O were
- introduced in HIV-1 M gag-pol and HIV-1 M CYPA binding loop was transferred to HIV-1
- 710 N and HIV-1 O *gag-pol*. These CYPA loop mutants were then used to infect WT or TRIM5α
- 711 KO U-87 MG cells for two to three days, Luciferase activity was measured, infection of KO

cells was normalized to infection of WT cells. All experiments were repeated for a minimum of three times.

Fig. 2. Capsid residues 88 and 89 mediates susceptibility to huTRIM5α. (A, B) A88V and G89V capsid mutations for HIV-1 M, (C, D) V88A for HIV-1 N, M88A for HIV-1 O and V88A mutation for HIV-1 P were introduced in their respective *gag-pol* constructs. WT and capsid mutants were tested in infections of WT or TRIM5α KO U-87 MG cells. Infection of mutant viruses was normalized to infection of corresponding WT virus. (E) GST-pulldown of CYPA (CYPA-GST) with capsid proteins of HIV-1 M, N, O or P. GST: GST not fused to CYPA. Viral lysates and GST-tagged CYPA protein lysates were specifically incubated together with GST Sepharose beads. The eluate was subjected to immunoblotting to detect viral p24 (capsid) and GST-tagged CYPA (pulldown). Cell and viral lysates were also loaded as inputs for GST-tagged CYPA and p24, respectively. (F) Immunoblot of viral particles and corresponding virus producer cells. The level of CYPA packaged by virions was analyzed by anti-HA staining (for CYPA-HA), virus was confirmed by anti-p24 (capsid) antibody staining, anti-tubulin was used to confirm equal amounts of cell lysates loaded. Cells were treated with cyclosporine A (CsA) from 0 to 2.5 μM. (G) The amount of packaged CYPA in relation to the used CsA dose was quantified using ImageJ.

Fig. 3. Cyclophilin A binds to the CYPA binding loop of HIV-1 M capsid, where it can exert cis/trans isomerase activity at the G89-P90 ω dihedral (36) (A) Overview of the simulated complex. CYPA (shown in gray) binds to the CYPA binding loop (orange) on the surface of the HIV-1 capsid. Monomers are colored differently; the region in the black box is shown as a blowup in panel (B). (B) Close-up view of the CYPA binding loop. The ω dihedral between residues G89 and P90 (shown as sticks) is marked, evaluated as the angle between the normals on the planes formed by the atoms ($C_a(G89)$, C(G89), N(P90)) and (C(G89), N(P90), $C_{\alpha}(P90)$). (C) Potential of mean force (free energy profile) along the ω dihedral of G89-P90 in HIV-1 M wild type with or without CYPA. The height of the energy barrier for the transition from the trans (180°) to the cis (0°) conformation is marked with a black line. HIV-1 M capsid without CYPA (red triangle) has a higher isomerization barrier than HIV-1 M bound to CYPA (orange triangle). The height of the free energy difference between trans (180°) and cis (0°) conformation is marked with a grey line. HIV-1 M capsid without CYPA (red circle) has a lower free energy difference than HIV-1 M bound to CYPA (orange circle). (D) Barrier heights ($\Delta G_{t,c}^{\#}$, triangles) and free energy differences ($\Delta G_{t,c}$, circles) from the potential of mean force computations for the cis/trans isomerization of the ω angle between G89 and P90 (Fig. S4). The HIV-1 types and variants are sorted from top to bottom according to the decrease in $\Delta G_{t_{\Delta c}}^{\#}$ in the presence of CYPA.

Fig. 4. Wildtype, N66D, H69R or N66D-H69R mutations in CYPA domain of rhTRIMCyp or capsid mutations at position 88 affect rhTRIMCyp antiviral activity in a virus-dependent way. (A) Immunoblot of CrFK cells expressing rhTRIMCyp or its mutants with N66D (rhTRIMCyp.N66D) or H69R (rhTRIMCyp.H69R) or N66D-H69R (rhTRIMCyp.N66D.H69R). (B, C) CrFK cells expressing WT or mutated rhTRIMCyps were infection by luciferase reporter viruses from HIV-1 M, N, O or P or their capsid mutants at position 88. Two to three days after infection, cells were lysed, and luciferase activity was measured. Infectivity of each virus on control cells expressing the empty vector (vector) were used as reference. NH: rhTRIMCyp with N66 and H69 in CYPA domain, DH: rhTRIMCyp with N66D mutation in CYPA, NR: rhTRIMCyp with H69R mutation in CYPA, DR:

rhTRIMCyp with N66D and H69R mutations in CYPA. All experiments were done at least three times in triplicates.

Fig. 5. CYPA knockdown (KD) and CYPA, TRIM5α double depletion differentially affect infection by HIV-1 M, N, O and P. (A) Immunoblot of CYPA KD in WT and in TRIM5α knockout (KO) U-87 MG cells. CYPA expression was detected by anti-CYPA antibodies and GAPDH detection served as control for equal protein loading. (B-E) WT and TRIM5α, CYPA, and double KO U-87 MG cells were infected by HIV luciferase reporter viruses from different groups M, N, O or P for 48 to 72 hrs and luciferase activity was measured. Infection of mutated cells were normalized to infection of WT (vector) cells. (F-I) HIV luciferase reporter viruses from groups M, N, O or P infection, in the presence of increasing amounts of cyclosporine A (CsA), of (F) WT U-87 MG cells, (G) CYPA KD U-87 MG cells, (H) TRIM5α KO U-87 MG cells, and (I) CYPA KD - TRIM5α KO U-87 MG cells. Two to three days later, luciferase activity was assessed, and data analysis was done in comparison to control infection. All experiments were repeated at least three times independently with similar findings.

Fig. 1 kDa α -TRIM5 α 55-40- $\alpha\text{-}\mathsf{GAPDH}$ В 700 D pMDLg/pRRE (HIV-1 M) pMDLg/pRRE.HIV-1 N CA HIV-1 M
HIV-1 N
HIV-1 O
HIV-1 P SIVcpzPts
SIVcpzPtt
EIAV pMDLg/pRRE.HIV-1 O CA 600-700 % of control infection % of control infection pMDLg/pRRE.HIV-1 P CA 600 500 300 WT KO wт WT KO KO C LTR Pol LTR Gag Env HIV-1 N HIV-1 O Non-M 7 Capsid HIV-1 P HIV-1 M HIV-1 M.N loop HIV-1 M.O loop HIV-1 O
HIV-1 N
HIV-1 N.M loop
HIV-1 O.M loop 500-Gag Pol HIV-1 M control infection (pMDLg/pRRE) Capsid CYPA loop 200of Q WT KO WT KO WT KO WT KO WT KO WT KO

Fig. 2 C D 500 120-500 450-100-450 % of control infection % of control infection % of control infection 400 % of control infection 400 350 350 80-300 300 250 250 60-200 200 40-40-150 150 100 100 20-20-N 1884 N **188A** N N88A N N88A Nr. M 1884 188F HIV-1 N HIV-1 O HIV-1 P HIV-1 M HIV-1 O HIV-1 M HIV-1 P HIV-1 N TRIM5 α KO U-87 MG cells Wild type U-87 MG cells WT U-87 MG cells $TRIM5\alpha$ KO U-87 MG cells No virus Ε HIV-1 O HIV-1 M HIV-1 N HIV-1 P **GS7** 0.5 1 2.5 μM CsA 2.5 kDa 25kDa 55 CYPA-GST α -HA α-GST ▮ Virus Pulldown 25 α -p24 25 α-p24 α-ΗΑ 55 α-GST Cells Input 55-25 α-p24 α -tubulin G 1103 DMSO % of packaged CYPA ■ 0.5 µM CsA 1 μM CsA 2.5 µM CsA HIV-1 N

HIV-1 O

HIV-1 P

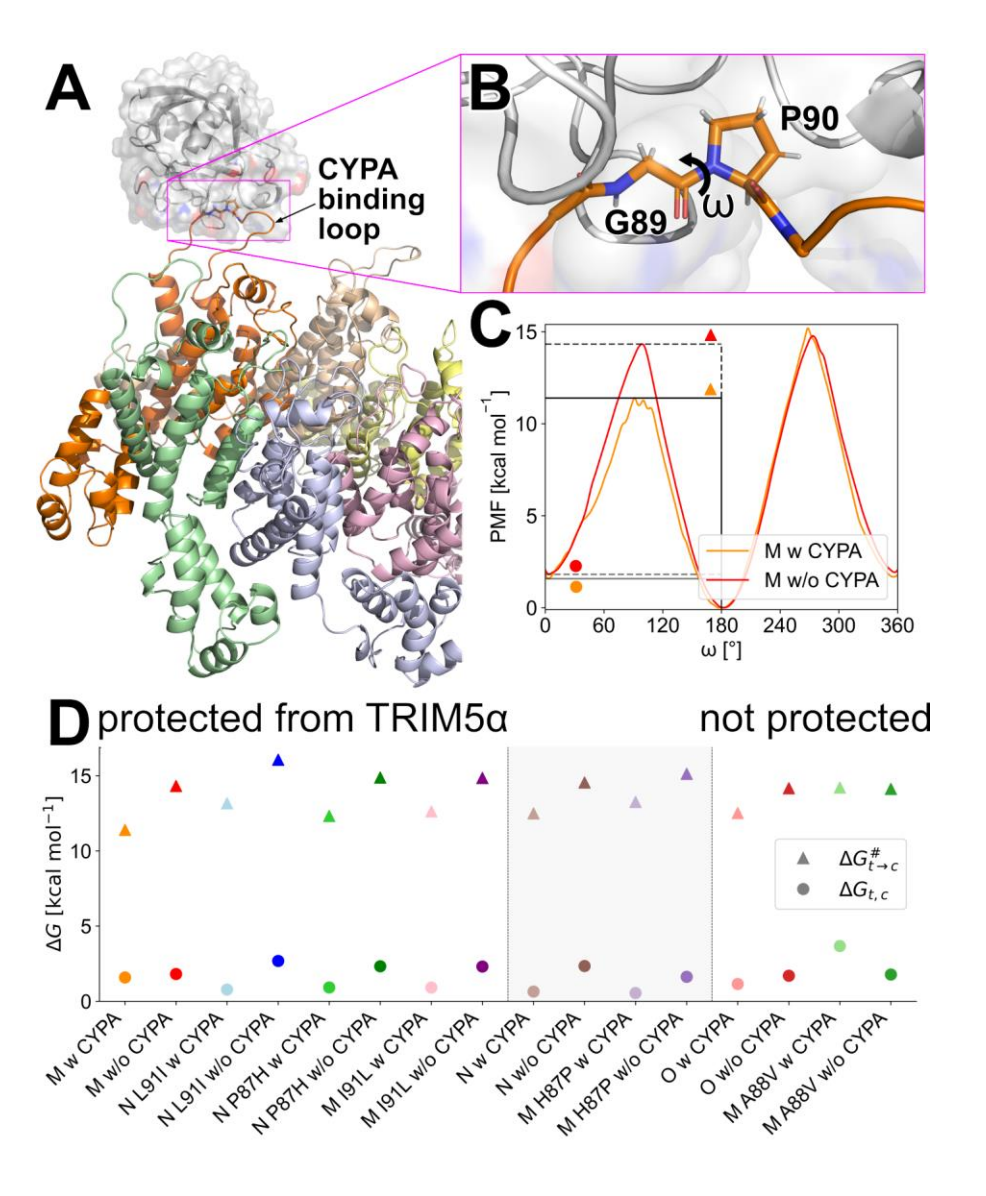


Fig. 4

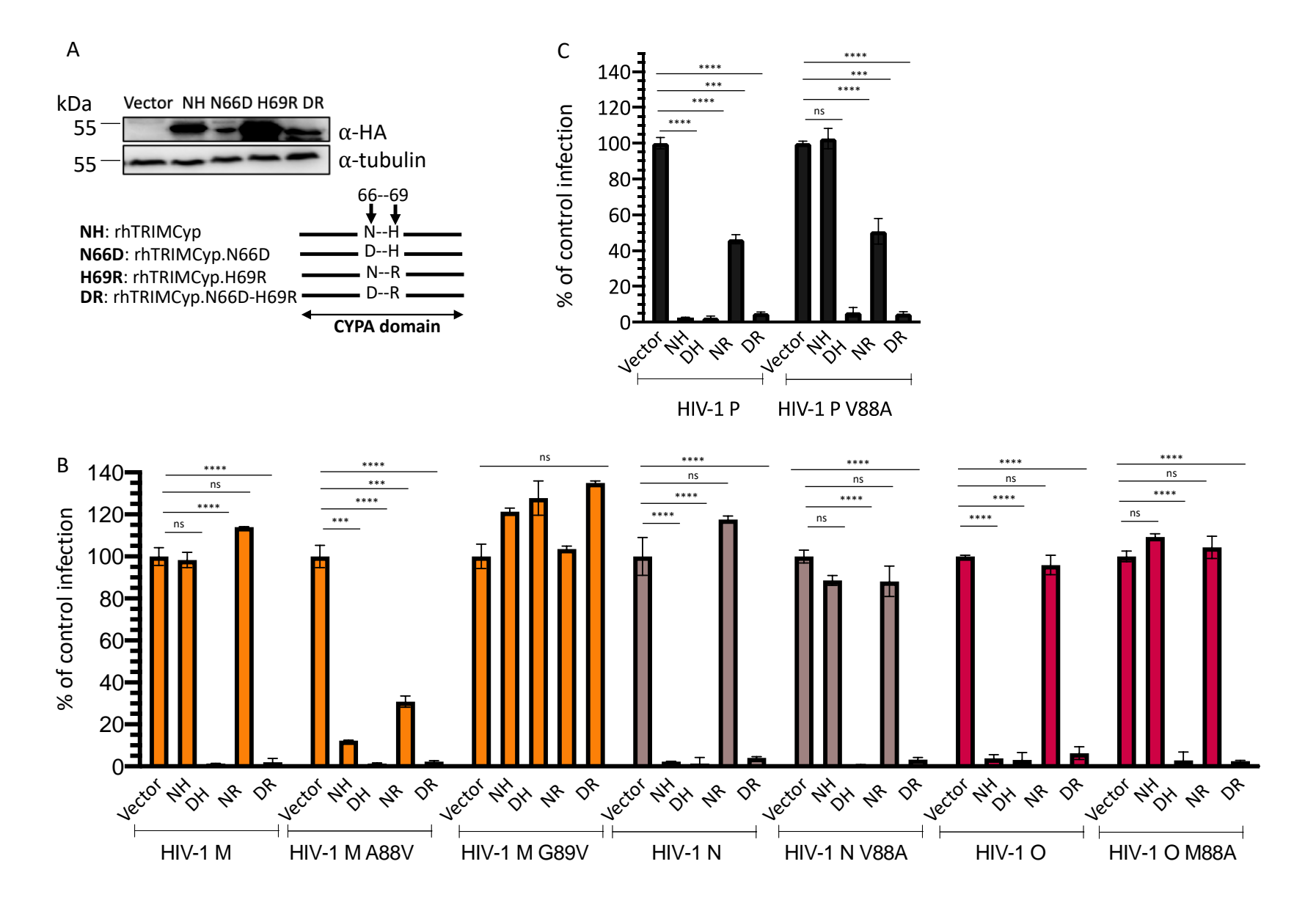


Fig. 5

